**Effect of diffusivity of amyloid beta monomers on the formation of senile plaques**

Andrey V. Kuznetsov

Department of Mechanical and Aerospace Engineering, North Carolina State University,

Raleigh, NC 27695-7910, USA; e-mail: avkuznet@ncsu.edu

**Abstract**

Alzheimer's disease (AD) presents a perplexing question: why does its development span decades, even though individual amyloid beta (Aβ) deposits (senile plaques) can form rapidly in as little as 24 hours, as recent publications suggest? This study proposes a hypothesis that the formation of senile plaques is not limited by polymerization kinetics. Instead, their formation appears to be limited by the diffusion-driven supply of Aβ monomers, along with the rate at which the monomers are produced from amyloid precursor protein (APP) and the rate at which Aβ monomers undergo degradation. A mathematical model incorporating the nucleation and autocatalytic process (via the Finke-Watzky model), as well as Aβ monomer diffusion, was proposed. The obtained system of partial differential equations was solved numerically, and a simplified version was investigated analytically. The computational results predicted that it takes approximately 7 years for Aβ aggregates to reach a neurotoxic concentration of 50 μM. Additionally, a sensitivity analysis was performed to examine how the diffusivity of Aβ monomers and their production rate impact the concentration of Aβ aggregates.

**Keywords:** neuron; Alzheimer's disease; Finke−Watzky model, mathematical modeling; neurotoxicity; polymerization

**Abbreviations**

| | |
|---|---|
| Aβ | amyloid beta |
| AD | Alzheimer's disease |
| CV | control volume |
| F-W | Finke-Watzky |

## 1. Introduction

Alzheimer's disease (AD) is a severe neurodegenerative disorder and the leading cause of dementia [1-3]. One characteristic hallmark of AD is the spontaneous aggregation of amyloid peptides into fibrillar aggregates, which is aided by an autocatalytic process known as secondary nucleation [4]. The presence of accumulating Aβ deposits (senile plaques) in the brains of Alzheimer's disease (AD) patients is a well-established fact, regardless of whether they are causative agents of the disease or simply serve as markers for it [5-7]. Aβ monomers are produced by β- and γ-secretase cleavage of amyloid precursor protein (APP), which is synthesized in neurons [6,8]. The majority of the Aβ monomers produced are released into the extracellular environment, where they have the potential to aggregate [9].

Numerous studies have provided evidence of a link between the spread of amyloidogenic proteins and neurodegenerative diseases, including AD, Parkinson's disease, Huntington's disease, and Amyotrophic Lateral Sclerosis [10,11]. In a study conducted by [12], the Finke-Watzky (F-W) two-step model was utilized to curve-fit published data on amyloid-beta (Aβ) aggregation, obtained from studies by [13,14]. Typically, the data are presented for two isoforms, Aβ40 and Aβ42, with the latter being more prone to aggregation.

Senile plaques in patients with AD accumulate over many years. Interestingly, a study conducted in [15] revealed that individual plaques can actually form quite rapidly, within approximately 24 hours. To understand this apparent paradox, this investigation explored the role of Aβ monomer diffusion in the process of Aβ aggregate formation. The proposed hypothesis states that the slow diffusion of Aβ, along with the limited rate of synthesis of Aβ monomers, can be contributing factors to the gradual formation of senile plaques. Thus, it is proposed that the rate of plaque formation is influenced not only by the kinetics of their growth but also by the rate at which the essential reactants (Aβ monomers) are produced and supplied through diffusion, and also by the rate at which Aβ monomers are destroyed by the proteolytic system.

Mathematical models aimed at understanding the intraneuronal mechanisms leading to the formation of amyloid-β plaques were developed in [16-18]. However, these earlier studies mainly focused on simulating intracellular processes and did not consider the extracellular diffusion of Aβ monomers, which is an important process to consider since Aβ monomers are easily diffusible. The current research builds upon the previous models and specifically investigates the diffusion of Aβ monomers in the extracellular space and its impact on the formation of Aβ aggregates.

## 2. Materials and models

### 2.1. Model equations

The F-W model is a simplified two-step process that describes the formation of certain aggregates. It involves two pseudo-elementary reaction steps: nucleation and autocatalysis. In the nucleation step, there is a continuous formation of new aggregates, while in the autocatalysis step, the surface growth of these aggregates occurs rapidly [12,19]. The two pseudo-elementary reaction steps are

$$A \xrightarrow{k_1} B\,, \tag{1}$$

$$A + B \xrightarrow{k_2} 2B\,, \tag{2}$$

where $A$ denotes a monomeric protein, and $B$ denotes an amyloid-converted protein. Kinetic constants $k_1$ and $k_2$ represent the rates of nucleation and autocatalytic growth, respectively [12]. The primary nucleation process, described by Eq. (1), exclusively involves monomers. In contrast, secondary nucleation, described by Eq. (2), involves both monomers and pre-existing aggregates of the same peptide [4].

In this study, the F-W model is employed to simulate the conversion of monomers, with a concentration denoted as $C_A$, into aggregates, represented by $C_B$. These aggregates encompass various forms of Aβ oligomers, protofibrils, and fibrils [20]. The formation of Aβ aggregates is responsible for the deposition of amyloid plaques. Note that the minimalistic nature of the F-W model does not allow it to distinguish between different types and sizes of aggregates. Typically, the F-W model is used to investigate the conversion of a given initial concentration of monomers into aggregates. In this work, a novel extension of the F-W model is proposed to handle scenarios where monomers are continuously supplied through diffusion from the left-hand side of the system, represented by the position $x$=0. At the boundary $x$=0, which could simulate such a location as the cellular membrane [21,22], Aβ monomers are generated through the cleavage of APP (amyloid precursor protein). The boundary at $x$=$L$ corresponds to an extracellular location. The model proposed in this paper thus is

$$\frac{\partial C_A}{\partial t} = D_A \frac{\partial^2 C_A}{\partial x^2} - k_1 C_A - k_2 C_A C_B - C_A \frac{\ln(2)}{T_{1/2,A}}\,, \tag{3}$$

$$\frac{\partial C_B}{\partial t} = k_1 C_A + k_2 C_A C_B\,. \tag{4}$$

The initial conditions are as follows:

At $t=0$: $C_A=0$, $C_B=0$. (5a,b)

The boundary conditions are as follows:

At $x=0$: $D_A \frac{\partial C_A}{\partial x} = q_{A,0}$. (6)

At $x=L$: $\frac{\partial C_A}{\partial x} = 0$. (7)

Eqs. (6) and (7) assume that Aβ monomers are released from the boundary located at $x$=0. The boundary at $x$=$L$ is modeled as a symmetric one, as it corresponds to a half distance between senile plaques. Therefore, no flux of Aβ monomers occurs through this boundary.

The independent variables used in the model are listed in Table 1, and the dependent variables are summarized in Table 2. Table 3 provides a summary of the parameters utilized in the model.

Table 1. Independent variables used in the model.

| Symbol | Definition | Units |
|---|---|---|
| $t$ | Time | s |
| $x$ | Linear coordinate measuring the distance from the face of the CV through which Aβ monomers are supplied | μm |

Table 2. Dependent variables used in the model.

| Symbol | Definition | Units |
|---|---|---|
| $C_A$ | Molar concentration of Aβ monomers | μM |
| $C_B$ | Molar concentration of Aβ aggregates | μM |

Table 3. Parameters used in the model and the discussion of its results.

| Symbol | Definition | Units | Value or range | Reference or estimation method | Value(s) used in computations |
|---|---|---|---|---|---|

| | | | | | |
|---|---|---|---|---|---|
| $C_{A,0}$ | Initial concentration of Aβ monomers | μM | $0.25\times10^{-3}$ - $0.425\times10^{-3}$ [a] | [23] | |
| $C_{B,tox}$ | Neurotoxic concentration of Aβ oligomers | μM | 50 [b] | [24] | |
| $D_A$ | Diffusivity of Aβ monomers | $\mu m^2/s$ | 62.3 [c] | [23] | 62.3 |
| $k_1$ | Rate constant for the first pseudo-elementary step of the F-W model, which describes the nucleation of Aβ aggregates | $s^{-1}$ | $2.22\times10^{-9}$ [d] | [12,13] | $2.22\times10^{-9}$ |
| $k_2$ | Rate constant for the second pseudo-elementary step of the F-W model, which describes the autocatalytic growth of Aβ aggregates | $\mu M^{-1}\ s^{-1}$ | $9.44\times10^{-6}$ [d] | [12,13] | $9.44\times10^{-6}$ |
| $L$ | Half distance between senile plaques | μm | 50 | Estimated from Fig. 1a in [25] | 50 |
| $q_{A,0}$ | Flux of Aβ monomers from left-hand side boundary of the CV with a volume $L^3$ | $\mu M\ \mu m\ s^{-1}$ | $1.1\times10^{-5}$ [e] | [24] | $1.1\times10^{-5}$ |

| | | | | | |
|---|---|---|---|---|---|
| $T_{1/2,A}$ | Half-life of Aβ monomers | s | $4.61\times10^{3}$ [f] | [23] | $4.61\times10^{3}$, $4.61\times10^{9}$ (to represent $T_{1/2,A}\to\infty$) |

[a] The parameter ranges from 250 pM to 425 pM, as reported in [23]. Although this parameter is not directly involved in the model, it has been included in the table because it plays a role in discussing the concentration of Aβ monomers predicted by the model.

[b] The value corresponds to the Aβ42 isoform [24]. While this parameter is not directly involved in the model, it is included in the table because it is relevant for discussing the model's predictions regarding the time it takes for Aβ aggregates to reach the neurotoxic concentration.

[c] The diffusivity value is $0.623\times10^{-6}$ cm$^2$/s [23]. This value is smaller than the one reported in [26] ( $1.43\times10^{-6}$ cm$^2$/s) because the estimate reported in [23] takes into account the effect of tortuosity. Tortuosity accounts for the reduction of diffusion in brain tissue caused by various barriers, such as cells and the extracellular matrix.

[d] Values reported in [12] were obtained by curve-fitting data from [13]. $k_1 = 8\times10^{-6}$ h$^{-1}$, $k_2 = 3.4\times10^{-2}$ μM$^{-1}$ h$^{-1}$ [12].

[e] According to [24], the human brain produces Aβ42 monomers at a rate of $0.33\times10^{-6}$ μmol s$^{-1}$. Considering the approximate volume of the brain as $1.5\times10^{15}$ μm$^3$, the rate of Aβ42 production per unit volume is estimated to be $2.2\times10^{-22}$ μmol μm$^{-3}$ s$^{-1}$. In a small cube with a side length of $L$ (representing the CV in Fig. 1), the rate of Aβ42 production is $2.75\times10^{-17}$ μmol s$^{-1}$. Production of Aβ monomers occurs at the lipid membrane [27]. Assuming that all Aβ42 is released from the left-hand side face of the cube with an area of $L^2$, the rate of Aβ42 release per unit area is $1.1\times10^{-20}$ μmol μm$^{-2}$ s$^{-1}$ $=1.1\times10^{-5}$ μM μm s$^{-1}$.

[f] According to [23], the value is 1.28 hours.

The dimensionless form of Eqs. (3)-(7) is given in section S1.1 in Supplementary Materials. Aβ aggregation process is governed by three dimensionless parameters: (1) a parameter that defines the diffusivity of Aβ monomers, $D_A^* = D_A / \left(L^2 k_1\right)$; (2) a parameter that characterizes the rate at which Aβ

monomers are produced, $q_{A,0}^{*} = q_{A,0}k_2 / \left(k_1^2 L\right)$; (3) a parameter that characterizes the half-life of Aβ monomers, $T_{1/2,A}^{*} = T_{1/2,A}k_1$.

A negligible variation in $C_A$ along $x$ implies that the diffusion of Aβ monomers is infinitely fast. One of the supporting arguments for this assumption is that if the soluble Aβ diffuses slower than the speed of aggregation, growth will happen at the aggregate's tips, resulting in a ramified tree-like structure, which contrasts with the experimental observations [28]. Under this assumption, the control volume (CV) shown in Fig. 1 can be treated as a lumped capacitance body and Eqs. (3) and (4) can be reformulated as follows:

$$\frac{dC_A}{dt} = -k_1 C_A - k_2 C_A C_B - C_A \frac{\ln(2)}{T_{1/2,A}} + \frac{q_{A,0}}{L}, \tag{8}$$

$$\frac{dC_B}{dt} = k_1 C_A + k_2 C_A C_B. \tag{9}$$

The dimensionless forms of Eqs. (8) and (9) are given in section S1.2 in Supplementary Materials. Upon adding Eqs. (8) and (9), we obtain the following result:

$$\frac{dC_A}{dt} + \frac{dC_B}{dt} = -C_A \frac{\ln(2)}{T_{1/2,A}} + \frac{q_{A,0}}{L}. \tag{10}$$

For the case of $T_{1/2,A} \to \infty$, integrating Eq. (10) with respect to time and using the initial condition given by Eq. (5a,b), the following result is obtained:

$$C_A + C_B = \frac{q_{A,0}}{L} t. \tag{11}$$

The increase of $C_A + C_B$ with time is attributed to the supply of Aβ monomers through the left-hand side boundary of the CV. By eliminating $C_A$ from Eq. (4) using Eq. (11), the following is obtained:

$$\frac{dC_B}{dt} = k_1 \left( \frac{q_{A,0}}{L} t - C_B \right) + k_2 \left( \frac{q_{A,0}}{L} t - C_B \right) C_B. \tag{12}$$

Eq. (12) is similar to the one studied in [29]. To find the exact solution of Eq. (12) with the initial condition given by Eq. (5b), the DSolve function followed by the FullSimplify function in Mathematica 13.3 (Wolfram Research, Champaign, IL) was employed. The resulting solution is as follows:

$$C_B = \frac{k_1}{k_2}$$

$$\times\left(-1+\frac{\left(k_2 q_{A,0}\right)^{1/2}\exp\left[k_1 t+\frac{k_2 q_{A,0}}{2L}t^2\right]}{\left(k_2 q_{A,0}\right)^{1/2}-\left(2L\right)^{1/2}k_1\left(F\left(\frac{k_1 L^{1/2}}{\left(2k_2 q_{A,0}\right)^{1/2}}\right)\right)-\exp\left[k_1 t+\frac{k_2 q_{A,0}}{2L}t^2\right]F\left[\frac{k_1 L+k_2 q_{A,0}t}{\left(2k_2 q_{A,0}L\right)^{1/2}}\right]}\right). \quad (13)$$

In this equation, $F(x)$ is Dawson's integral:

$$F(x)=\frac{1}{2}\sqrt{\pi}\,e^{-x^2}erfi(x), \quad (14)$$

where $erfi(x)$ is the imaginary error function.

$C_A$ can then be found using Eq. (11) as:

$$C_A = \frac{q_{A,0}}{L}t - C_B\,. \quad (15)$$

The exact solution provided by Eqs. (13) and (15) is quite cumbersome. A more elegant approximate solution, also valid for the case of $T_{1/2,A}\to\infty$, is

$$C_A = \frac{\frac{q_{A,0}}{L}}{k_1 + k_2\frac{q_{A,0}}{L}t}, \quad (16)$$

$$C_B = \frac{q_{A,0}}{L}t\,. \quad (17)$$

Note that as $t\to\infty$, Eq. (16) predicts that $C_A\to 0$. The dimensionless forms of Eqs. (16) and (17) are given in section S1.3 in Supplementary Materials.

**2.2. Sensitivity analysis**

One of the main objectives of this study was to investigate the sensitivity of Aβ aggregate concentration to the diffusivity of Aβ monomers. The sensitivity of the concentration of Aβ aggregates to the rate of Aβ monomer production, which is characterized by $q_{A,0}$, was also investigated.

This was done by calculating the local sensitivity coefficients, which represent the first-order partial derivatives of the observable (the concentration of Aβ aggregates) with respect to the diffusivity of Aβ monomers or the flux of Aβ monomers entering the CV through the left-hand side boundary, following [30-33]. The calculation of the sensitivity coefficient of $C_B$ to (for example) $D_A$ was performed as follows:

$$\frac{\partial C_B}{\partial D_A} \approx \left. \frac{C_B\left(D_A + \Delta D_A\right) - C_B\left(D_A\right)}{\Delta D_A} \right|_{\text{other parmeters kept constant}}, \tag{18}$$

where $\Delta D_A = 10^{-3} D_A$ is the step size. Calculations were performed using different step sizes to test the independence of the sensitivity coefficients of the step size.

The non-dimensionalized relative sensitivity coefficient was calculated following [31,34] as, for example:

$$S_{D_A}^{C_B} = \frac{D_A}{C_B} \frac{\partial C_B}{\partial D_A}. \tag{19}$$

**S3. Numerical solution**

Eqs. (3) and (4) form a system of two partial differential equations (PDEs). They were solved subject to initial conditions given by Eq. (5) and boundary conditions given by Eqs. (6) and (7) using MATLAB's PDEPE solver (MATLAB R2020b, MathWorks, Natick, MA, USA). MATLAB's ODE45 solver was used to solve Eq. (12) with initial condition (5b) (for large values of *t*, using MATLAB's solver works better than the analytical solution given by Eq. (13)). To ensure accurate results, the error tolerance parameters, RelTol and AbsTol, were set to 1e-10.

**3. Results**

Figs. 2 and 3 depict the scenario where the half-life of Aβ monomers is assumed to be infinite. In Fig. 2a, the concentration of Aβ monomers is approximately $0.465 \times 10^{-3}$ μM, which is close to the range reported in [23] (Table 3): $0.25 \times 10^{-3}$ to $0.425 \times 10^{-3}$ μM. The concentrations of monomers, $C_A$, and aggregates,

$C_B$, gradually decrease from $x$=0 to $x$=$L$. This decline occurs due to monomer diffusion from the boundary where monomers are supplied ($x$=0), leading to the highest concentration, to the boundary with a symmetric (zero flux) boundary condition ($x$=$L$), where both Aβ monomer and aggregate concentrations are at their lowest (Figs. 2a and 2b). Note that in this case, the concentration of aggregates reaches the neurotoxic level of 50 μM (Fig. 2b) within the timescale of $t = 7.23$ years.

Initially, at the right-hand side boundary of the CV, $x = L$, the concentration of Aβ monomers is zero, as indicated by the initial condition in Eq. (5a). Subsequently, it rapidly increases, followed by a decline, and then stabilizes at a low level due to the conversion of monomers into aggregates (Fig. 3a). The concentration of aggregates steadily increases in a linear fashion owing to the continuous supply of reactants (monomers) through the left-hand side boundary of the CV at $x$=0 (Fig. 3b). When the diffusivity of the monomers is decreased, the concentration of aggregates exhibits a slightly slower increase, as illustrated by the red solid curve in Fig. 3b corresponding to $D_A = 6.23$ μm²/s.

To gain a deeper understanding of how the concentrations of Aβ monomers and aggregates evolve over time, we developed a simplified lumped capacitance model given by Eqs. (8) and (9). In Fig. S1, presented in the Supplementary Materials, we compared the numerical solution of Eqs. (8) and (9) for the case of $T_{1/2,A} \to \infty$ with the approximate analytical solution provided by Eqs. (16) and (17). Remarkably, the approximate analytical solution of the lumped capacitance model shows excellent agreement with the numerical solution. As time progresses, the concentration of Aβ monomers decreases proportional to $\frac{1}{t}$ (Eq. (16)). This is consistent with the Finke-Watzky model, which disregards any potential equilibrium state between the monomers and aggregates, and predicts that the aggregation continues until all monomers are converted into aggregates [35,36]. The concentration of Aβ aggregates increases linearly with time (Eq. (17)). This is due to the reactants (Aβ monomers) entering the CV (Fig. 1) at a constant rate of $q_{A,0}L^2$; all reactants are subsequently converted into Aβ aggregates.

If the half-life of Aβ monomers is assumed to be finite, $T_{1/2,A} = 4.61 \times 10^3$ s (Figs. 4 and 5), the concentration of Aβ aggregates decreases significantly compared to the scenario with an infinite half-life, from approximately 50 μM to approximately $5.25 \times 10^{-3}$ μM (compare Fig. 4b with Fig. 2b). This notable decrease in the aggregate concentration occurs because, with a smaller half-life, a significant portion of the monomers is degraded by the proteolytic system rather than being converted into aggregates. This finding has significant implications for AD. Many studies have linked AD to the failure of the proteolytic

machinery to maintain low Aβ concentrations and to degrade faulty and misfolded Aβ [37-39]. The results obtained from this study suggest that Aβ aggregation can occur even under conditions of relatively low Aβ monomer concentration if the protein clearance machinery fails to continuously degrade newly produced normal monomers. Preventing Aβ aggregation thus requires more than just degrading faulty Aβ. Conversely, a properly functioning proteolytic machinery capable of degrading Aβ monomers can protect the brain from Aβ aggregates. Interestingly, to achieve this protection, the ability to degrade aggregates is not required (notably, there is no degradation term in Eq. (4)).

When simulating the scenario with a finite half-life of Aβ monomers, which corresponds to a well-functioning Aβ monomer clearance system, the initial peak in the concentration of Aβ monomers is absent (compare Fig. 5a with Fig. 3a). Furthermore, the increase in the concentration of Aβ aggregates, $C_B$, does not follow a linear trend and occurs much slower, ultimately reaching a significantly lower value after 7 years (compare Fig. 5b with Fig. 3b).

When the diffusivity of Aβ monomers, $D_A$, is increased, the concentration of Aβ monomers, $C_A$, initially exhibits an increase. However, once $D_A$ exceeds 30 μm²/s, $C_A$ reaches a plateau and remains constant even with further increases in $D_A$ (Fig. 6a). A similar trend is observed for the concentration of Aβ aggregates, $C_B$ (Fig. 6b).

Interestingly, in Fig. 6a, the concentration of Aβ monomers, $C_A$, for the scenario with an infinitely large half-life is higher than the concentration for the case with a finite half-life of Aβ monomers. It is important to note that the values of $C_A$ shown in Fig. 6a are not steady-state concentrations of monomers; the steady-state monomer concentration is zero (as indicated by Eq. (16)). Fig. 6a is computed for a specific time interval (*t* is changing between 0 and 7.23 years), and if time is increased further, the monomer concentrations for both infinite and finite half-life scenarios will eventually reduce to zero. In Fig. 6b, it is evident that the concentration of aggregates is larger for the scenario with an infinite half-life of monomers, which is consistent with expectations.

It is intriguing to note that in the scenario with an infinite half-life of Aβ monomers, the concentration of Aβ monomers, $C_A$, appears to be nearly independent of the rate of Aβ monomer production, $q_{A,0}$, as indicated by the horizontal solid red line in Fig. 7a. To investigate this further, a simplified model based on the lumped capacitance approximation was developed; this model is given by Eqs. (8) and (9). This model assumes a lack of concentration variations, of $C_A$ and $C_B$, with respect to *x*; it accounts for concentrations changing with time but not with the distance from the *x*=0 plane. Fig. S1a shows that $C_A$

becomes small after a short transient. Since the lumped capacitance model disregards the final value of Aβ monomer diffusivity, this suggests that $C_A$ is primarily determined by the Aβ monomer production rate and the conversion rate of Aβ monomers into aggregates. The concentration of Aβ aggregates, $C_B$, exhibits a linear increase with time (Fig. S1b). This is attributed to the rate of Aβ monomer production, $q_{A,0}$, remaining constant in the model and leading to the continuous conversion of Aβ monomers into aggregates. Similar trends can be observed in Fig. 3, where the finite rate of diffusion of Aβ monomers is taken into account.

As depicted in Fig. 7b, the concentration of Aβ aggregates, $C_B$, at the boundary $x=L$ (50 μm) and $t = 7.23$ years, increases linearly with $q_{A,0}$ at large times. This behavior is attributed to the fact that $q_{A,0}$ represents the rate at which reactants are produced and subsequently converted into Aβ aggregates. The production rate, $q_{A,0}$, is assumed to be constant and independent of time. The dimensionless sensitivity of the molar concentration of Aβ aggregates, $C_B$, to the diffusivity of Aβ monomers, $D_A$, remains consistently positive at all times $t$ (Fig. 8a). This is because Aβ monomers serve as reactants in the F-W model, which describes Aβ aggregation (Eqs. (1) and (2)). An increase in the diffusivity of monomers enhances the supply of reactants (see Figs. S2 and S3 in the Supplementary Materials, showing the flux of Aβ monomers), resulting in a greater accumulation of aggregated Aβ.

The dimensionless sensitivity of the concentration of Aβ aggregates, $C_B$, to the rate of Aβ monomer production, $q_{A,0}$, which enters the model through the flux of Aβ monomers from the left-hand side boundary, is also positive at all times $t$ (Fig. 8b). It is worth noting that in the scenario with an infinite half-life of Aβ monomers (represented by the red line in Fig. 8b), the sensitivity of $C_B$ to $q_{A,0}$ quickly stabilizes at a constant value of 1. This behavior is attributed to the linear dependence of $C_B$ on $q_{A,0}$ (as evident from the red solid line in Fig. 7b), indicating that $C_B$ is directly influenced by the rate of production of the reactants (Aβ monomers). The value of 1 in the sensitivity calculation is a result of rescaling in Eq. (19) that is performed to ensure that the dimensionless sensitivity is independent of magnitudes of parameters.

## 4. Discussion, limitations of the model, and future directions

One popular hypothesis associates sporadic forms of Alzheimer's disease (AD) with impaired clearance of Aβ aggregates [40-42]. The findings from this study suggest that preventing AD does not necessarily

require the proteolytic system to break down Aβ polymers. Instead, the results demonstrate that even if the proteolytic system only targets and degrades Aβ monomers, the aggregation of Aβ cannot progress due to the insufficient supply of reactants (monomers). This result holds significant implications for potential therapeutic interventions in AD.

The current model is limited as the F-W model it relies upon does not simulate the size of Aβ polymers. An enhanced model capable of simulating polymers with varying sizes would significantly enhance the value and accuracy of model predictions. Enhancing the model's accuracy would be possible with a more precise depiction of the CV's geometry, particularly focusing on the surface of the lipid membrane where Aβ monomers are generated.

In future research, it would be important to develop models that simulate the interaction between Aβ aggregates and tau tangles [8]. To achieve this, the model would need to account for cross-membrane diffusion processes, as Aβ aggregates are typically formed in the extracellular environment, while tau tangles are intracellular. Additionally, further modeling efforts should consider the activation of microglia in response to Aβ aggregation. It would be crucial to explore the potential combination of microglia-mediated degradation of Aβ aggregates and the neuroinflammatory response triggered by microglia activation [15,20,43].

**Acknowledgment**

AVK acknowledges the support provided by the National Science Foundation (grant CBET-2042834) and the Alexander von Humboldt Foundation through the Humboldt Research Award.

**References**


1. Hardy J. A hundred years of Alzheimer's disease research. *Neuron* 2006; **52**(1): 3-13.

2. Maqbool M, Mobashir M, Hoda N. Pivotal role of glycogen synthase kinase-3: A therapeutic target for Alzheimer's disease. *European Journal of Medicinal Chemistry* 2016; **107**: 63-81.

3. Hung S, Fu W. Drug candidates in clinical trials for Alzheimer's disease. *Journal of Biomedical Science* 2017; **24**: 47.

4. Thacker D, Barghouth M, Bless M, Zhang E, Linse S. Direct observation of secondary nucleation along the fibril surface of the amyloid β 42 peptide. *Proceedings of the National Academy of Sciences* 2023; **120**(25): e2220664120.

5. Hardy J, Selkoe DJ. The amyloid hypothesis of Alzheimer's disease: Progress and problems on the road to therapeutics. *Science (New York, N.Y.)* 2002; **297**(5580): 353-356.

6. O'Brien RJ, Wong PC. Amyloid precursor protein processing and Alzheimer's disease. *Annual Review of Neuroscience, Vol 34* 2011; **34**: 185-204.

7. Selkoe DJ, Hardy J. The amyloid hypothesis of Alzheimer's disease at 25years. *Embo Molecular Medicine* 2016; **8**(6): 595-608.

8. Hampel H, Hardy J, Blennow K, Chen C, Perry G, Kim SH, Villemagne VL, Aisen P, Vendruscolo M, Iwatsubo T, Masters CL, Cho M, Lannfelt L, Cummings JL, Vergallo A. The amyloid-β pathway in Alzheimer’s disease. *Molecular Psychiatry* 2021; **26**(10): 5481-5503.

9. Rahman MM, Lendel C. Extracellular protein components of amyloid plaques and their roles in Alzheimer’s disease pathology. *Molecular Neurodegeneration* 2021; **16**(1): 59.

10. Jucker M, Walker LC. Self-propagation of pathogenic protein aggregates in neurodegenerative diseases. *Nature* 2013; **501**(7465): 45-51.

11. Klimova N, Makarava N, Baskakov IV. The diversity and relationship of prion protein self-replicating states. *Virus Research* 2015; **207**: 113-119.

12. Morris AM, Watzky MA, Agar JN, Finke RG. Fitting neurological protein aggregation kinetic data via a 2-step, minimal/"Ockham's razor" model: The Finke-Watzky mechanism of nucleation followed by autocatalytic surface growth. *Biochemistry* 2008; **47**(8): 2413-2427.

13. Bieschke J, Zhang Q, Powers ET, Lerner RA, Kelly JW. Oxidative metabolites accelerate Alzheimer's amyloidogenesis by a two-step mechanism, eliminating the requirement for nucleation. *Biochemistry* 2005; **44**(13): 4977-4983.

14. Vestergaard M, Kerman K, Saito M, Nagatani N, Takamura Y, Tamiya E. A rapid label-free electrochemical detection and kinetic study of Alzheimer's amyloid beta aggregation. *Journal of the American Chemical Society* 2005; **127**(34): 11892-11893.

15. Meyer-Luehmann M, Spires-Jones TL, Prada C, Garcia-Alloza M, de Calignon A, Rozkalne A, Koenigsknecht-Talboo J, Holtzman DM, Bacskai BJ, Hyman BT. Rapid appearance and local toxicity of amyloid-beta plaques in a mouse model of Alzheimer's disease. *Nature* 2008; **451**: 720-724.

16. Kuznetsov IA, Kuznetsov AV. How the formation of amyloid plaques and neurofibrillary tangles may be related – A mathematical modelling study. *Proceedings of the Royal Society A* 2018; **474**: 20170777.

17. Kuznetsov IA, Kuznetsov AV. Simulating the effect of formation of amyloid plaques on aggregation of tau protein. *Proceedings of the Royal Society A-Mathematical Physical and Engineering Sciences* 2018; **474**(2220): 20180511.

18. Torok J, Maia PD, Verma P, Mezias C, Raj A. Emergence of directional bias in tau deposition from axonal transport dynamics. *PLOS Computational Biology* 2021; **17**(7): e1009258.

19. Iashchishyn IA, Sulskis D, Nguyen Ngoc M, Smirnovas V, Morozova-Roche LA. Finke-Watzky two-step nucleation-autocatalysis model of S100A9 amyloid formation: Protein misfolding as "nucleation" event. *ACS Chemical Neuroscience* 2017; **8**: 2152-2158.

20. Chen G, Xu T, Yan Y, Zhou Y, Jiang Y, Melcher K, Xu HE. Amyloid beta: Structure, biology and structure-based therapeutic development. *Acta Pharmacologica Sinica* 2017; **38**(9): 1205-1235.

21. Haass C, Kaether C, Thinakaran G, Sisodia S. Trafficking and proteolytic processing of APP. *Cold Spring Harbor Perspectives in Medicine* 2012; **2**(5): a006270.

22. Masters CL, Selkoe DJ. Biochemistry of amyloid β-protein and amyloid deposits in Alzheimer disease. *Cold Spring Harbor Perspectives in Medicine* 2012; **2**(6): a006262.

23. Waters J. The concentration of soluble extracellular amyloid-beta protein in acute brain slices from CRND8 mice. *PLOS One* 2010; **5**(12): e15709.

24. Raskatov JA. What is the "Relevant" amyloid β42 concentration? *ChemBioChem* 2019; **20**(13): 1725-1726.

25. Querol-Vilaseca M, Colom-Cadena M, Pegueroles J, Nuñez-Llaves R, Luque-Cabecerans J, Muñoz-Llahuna L, Andilla J, Belbin O, Spires-Jones T, Gelpi E, Clarimon J, Loza-Alvarez P, Fortea J, Lleó A. Nanoscale structure of amyloid-β plaques in Alzheimer's disease. *Scientific Reports* 2019; **9**(1): 5181.

26. Bora RP, Prabhakara R. Translational, rotational and internal dynamics of amyloid beta-peptides (A beta 40 and A beta 42) from molecular dynamics simulations. *Journal of Chemical Physics* 2009; **131**(15): 155103.

27. Dawkins E, Derks RJE, Schifferer M, Trambauer J, Winkler E, Simons M, Paquet D, Giera M, Kamp F, Steiner H. Membrane lipid remodeling modulates γ-secretase processivity. *Journal of Biological Chemistry* 2023; **299**(4)

28. Cruz L, Urbanc B, Buldyrev SV, Christie R, Gómez-Isla T, Havlin S, McNamara M, Stanley HE, Hyman BT. Aggregation and disaggregation of senile plaques in Alzheimer disease. *Proceedings of the National Academy of Sciences of the United States of America* 1997; **94**(14): 7612-7616.

29. Kuznetsov IA, Kuznetsov AV. An analytical solution simulating growth of lewy bodies. *Mathematical Medicine and Biology: A Journal of the IMA* 2022; **39**(3): 299-312.

30. Beck JV, Arnold KJ. *Parameter Estimation in Science and Engineering.* Wiley: New York, 1977.

31. Zadeh KS, Montas HJ. A class of exact solutions for biomacromolecule diffusion-reaction in live cells. *Journal of Theoretical Biology* 2010; **264**(3): 914-933.

32. Zi Z. Sensitivity analysis approaches applied to systems biology models. *IET Systems Biology* 2011; **5**(6): 336-346.

33. Kuznetsov IA, Kuznetsov AV. Investigating sensitivity coefficients characterizing the response of a model of tau protein transport in an axon to model parameters. *Computer Methods in Biomechanics and Biomedical Engineering* 2019; **22**(1): 71-83.

34. Kacser H, Burns JA, Fell DA. The control of flux. *Biochemical Society Transactions* 1995; **23**(2): 341-366.

35. Martin JD. Particle size is a primary determinant for sigmoidal kinetics of nanoparticle formation: A "disproof" of the Finke-Watzky (F-W) nanoparticle nucleation and growth mechanism. *Chemistry of Materials* 2020; **32**(8): 3651-3656.

36. Finke RG, Watzky MA, Whitehead CB. Response to "Particle size is a primary determinant for sigmoidal kinetics of nanoparticle formation: A "Disproof" of the Finke–Watzky (F-W) nanoparticle nucleation and growth mechanism". *Chemistry of Materials* 2020; **32**(8): 3657-3672.

37. Wang D, Dickson DW, Malter JS. Beta-amyloid degradation and Alzheimer's disease. *Journal of Biomedicine & Biotechnology* 2006; **2006**(3): 58406.

38. Baranello RJ, Bharani KL, Padmaraju V, Chopra N, Lahiri DK, Greig NH, Pappolla MA, Sambamurti K. Amyloid-beta protein clearance and degradation (ABCD) pathways and their role in Alzheimer's disease. *Current Alzheimer Research* 2015; **12**(1): 32-46.

39. Kim DE, Priefer R. Therapeutic potential of direct clearance of the amyloid-β in Alzheimer's disease. *Brain Sciences* 2020; **10**(2)

40. Selkoe DJ. Clearing the brain's amyloid cobwebs. *Neuron* 2001; **32**(2): 177-180.

41. Tanzi RE, Moir RD, Wagner SL. Clearance of Alzheimer's abeta peptide: The many roads to perdition. *Neuron* 2004; **43**(5): 605-608.

42. Saido T, Leissring MA. Proteolytic degradation of amyloid β-protein. *Cold Spring Harbor Perspectives in Medicine* 2012; **2**(6): a006379.

43. Hansen DV, Hanson JE, Sheng M. Microglia in Alzheimer's disease. *The Journal of Cell Biology* 2018; **217**(2): 459-472.

**Figure captions**

Fig. 1 A control volume (CV) with a width of $L = 50$ μm, employed to model the diffusion of Aβ monomers from the *x*=0 boundary and the accumulation of Aβ aggregates. The boundary at *x*=*L* is considered to be symmetric, resulting in no flux of Aβ monomers passing through it.

Fig. 2. The molar concentration of Aβ monomers, $C_A$, (a) and the molar concentration of Aβ aggregates, $C_B$, (b) as a function of the distance from the surface that releases Aβ monomers (e.g., cell membrane). These computational results are presented at $t = 2.28 \times 10^8 \text{ s} = 7.23 \text{ years}$ and correspond to the scenario with an infinite half-life of Aβ monomers.

Fig. 3. (a) Molar concentration of Aβ monomers, $C_A$, as a function of time (in years). (b) Molar concentration of Aβ aggregates, $C_B$, also as a function of time (in years). The computational results are presented at the right-hand side boundary of the CV, $x = L$. The scenario displayed in this figure assumes an infinite half-life of Aβ monomers.

Fig. 4. (a) Molar concentration of Aβ monomers, $C_A$, as a function of the distance from the surface that releases Aβ monomers (such as the cell membrane). (b) Molar concentration of Aβ aggregates, $C_B$, also as a function of the distance from the same surface. The computational results are presented at $t = 2.28 \times 10^8 \text{ s} = 7.23 \text{ years}$. The scenario displayed in this figure assumes a finite half-life of Aβ monomers ($T_{1/2,A} = 4.61 \times 10^3$ s).

Fig. 5. (a) Molar concentration of Aβ monomers, $C_A$, as a function of time (in years). (b) Molar concentration of Aβ aggregates, $C_B$, also as a function of time. The computational results are presented at the right-hand side boundary of the CV, $x = L$. The scenario displayed in this figure assumes a finite half-life of Aβ monomers ($T_{1/2,A} = 4.61 \times 10^3$ s).

Fig. 6. (a) Molar concentration of Aβ monomers, $C_A$, as a function of the diffusivity of Aβ monomers, $D_A$. (b) Molar concentration of Aβ aggregates, $C_B$, also as a function of the diffusivity of Aβ monomers, $D_A$. The computational results are presented at the right-hand side boundary of the CV, *x*=*L*, and at $t = 2.28 \times 10^8 \text{ s} = 7.23 \text{ years}$.

Fig. 7. (a) Molar concentration of Aβ monomers, $C_A$, as a function of the flux of Aβ monomers from the left-hand side boundary of the CV, $q_{A,0}$. (b) Molar concentration of Aβ aggregates, $C_B$, as a function of the flux of Aβ monomers from the right-hand side boundary of the CV, $q_{A,0}$. The computational results are presented at the boundary $x=L$ and $t = 2.28\times10^8 \text{ s} = 7.23 \text{ years}$.

Fig. 8. (a) Dimensionless sensitivity of the molar concentration of Aβ aggregates, $C_B$, to the diffusivity of Aβ monomers, $D_A$, as a function of time. (b) Dimensionless sensitivity of the molar concentration of Aβ aggregates, $C_B$, to the flux of Aβ monomers from the left-hand side boundary of the CV, $q_{A,0}$, also as a function of time. The computations were performed for $\Delta D_A = 10^{-3} D_A$ with a close result obtained for $\Delta D_A = 10^{-2} D_A$. The computational results are presented at the right-hand side boundary of the CV, $x = L$.

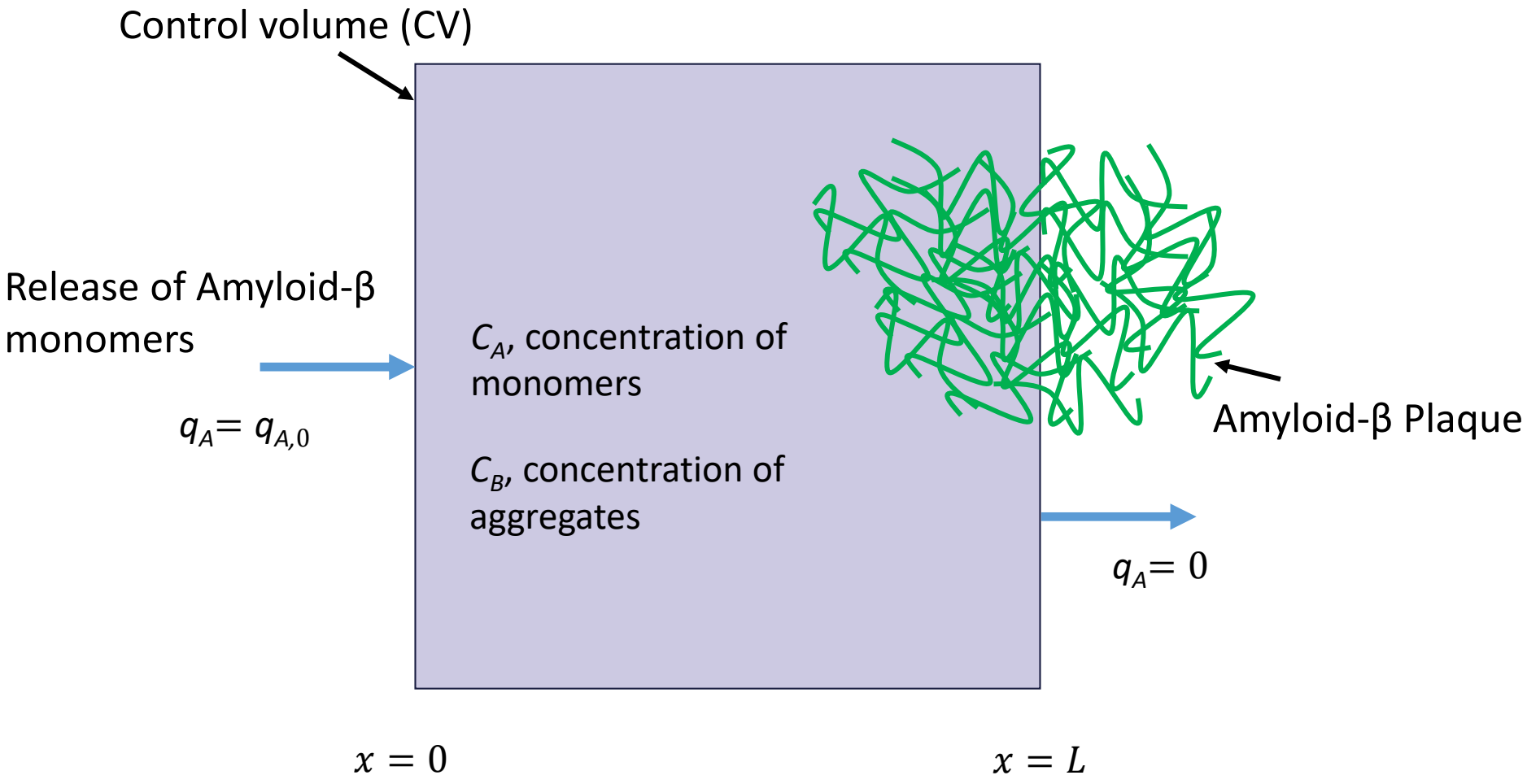
Control volume (CV)
Release of Amyloid-β monomers
$q_A = q_{A,0}$
$C_A$, concentration of monomers
$C_B$, concentration of aggregates
Amyloid-β Plaque
$q_A = 0$
$x = 0$
$x = L$

Figure 1

(a)

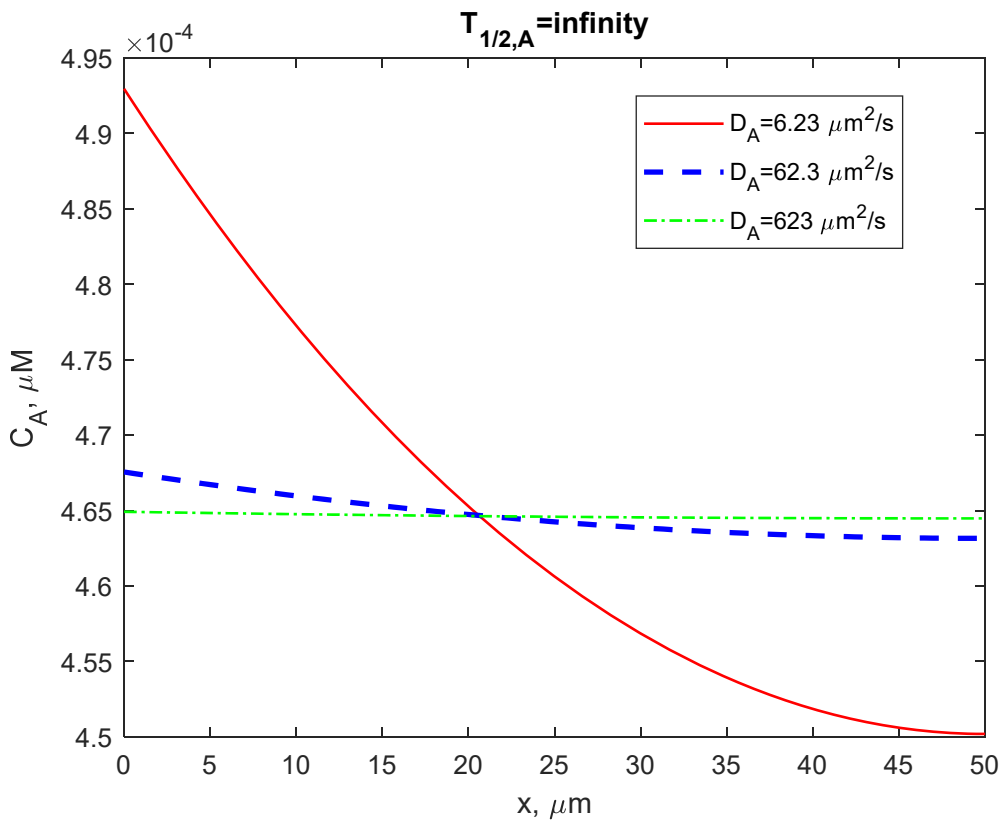
T1/2,A=infinity
×10-4
4.95
4.9
4.85
4.8
4.75
4.7
4.65
4.6
4.55
4.5
CA, μM
0
5
10
15
20
25
30
35
40
45
50
x, μm
DA=6.23 μm2/s
DA=62.3 μm2/s
DA=623 μm2/s

(b)

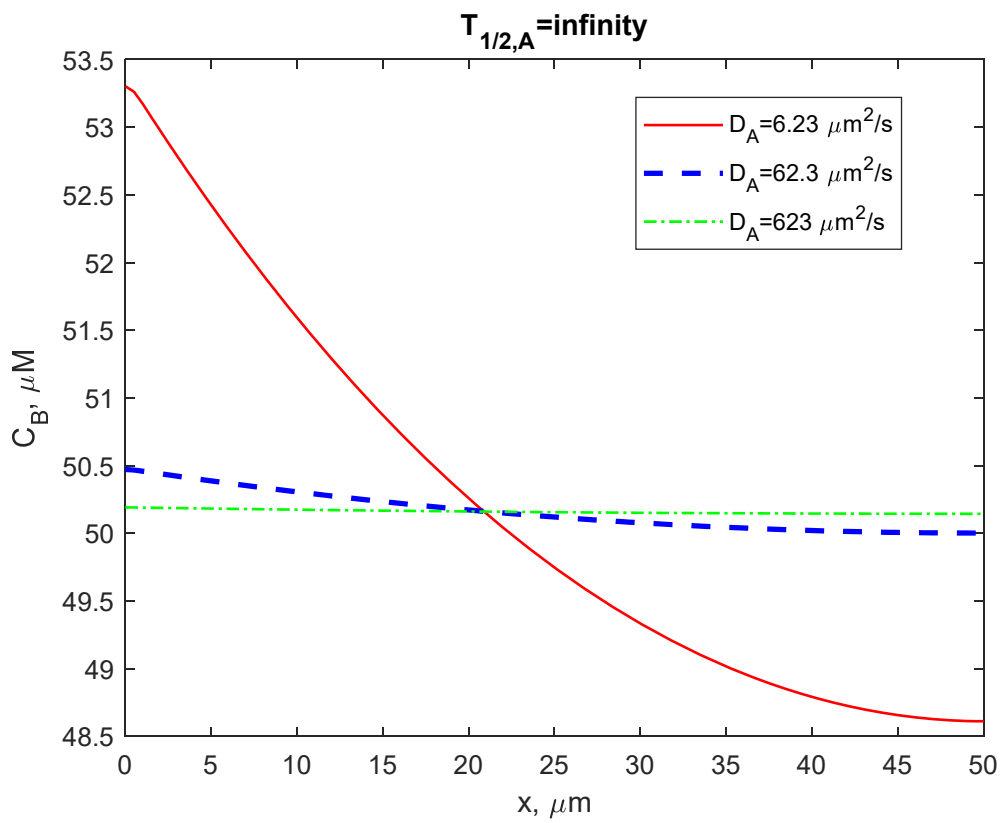
T1/2,A=infinity
53.5
53
52.5
52
51.5
51
50.5
50
49.5
49
48.5
CB, μM
0
5
10
15
20
25
30
35
40
45
50
x, μm
DA=6.23 μm2/s
DA=62.3 μm2/s
DA=623 μm2/s

Figure 2

(a)

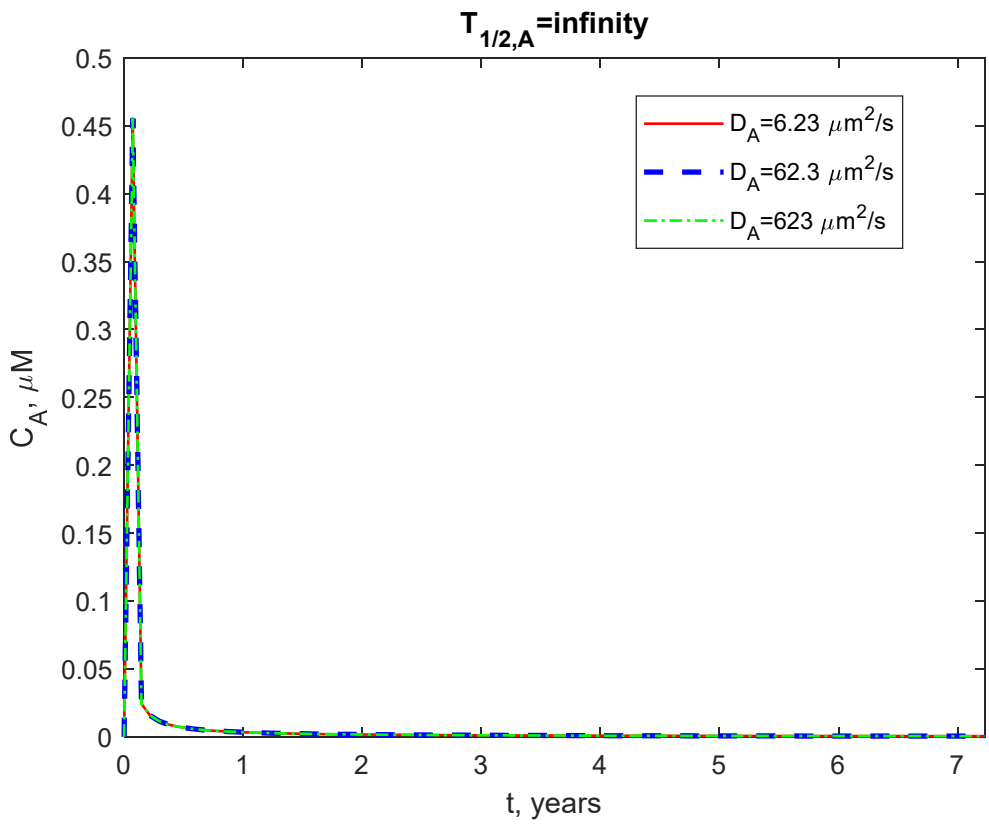
T1/2,A=infinity
0.5
0.45
0.4
0.35
0.3
0.25
0.2
0.15
0.1
0.05
0
CA, μM
0
1
2
3
4
5
6
7
t, years
DA=6.23 μm2/s
DA=62.3 μm2/s
DA=623 μm2/s

(b)

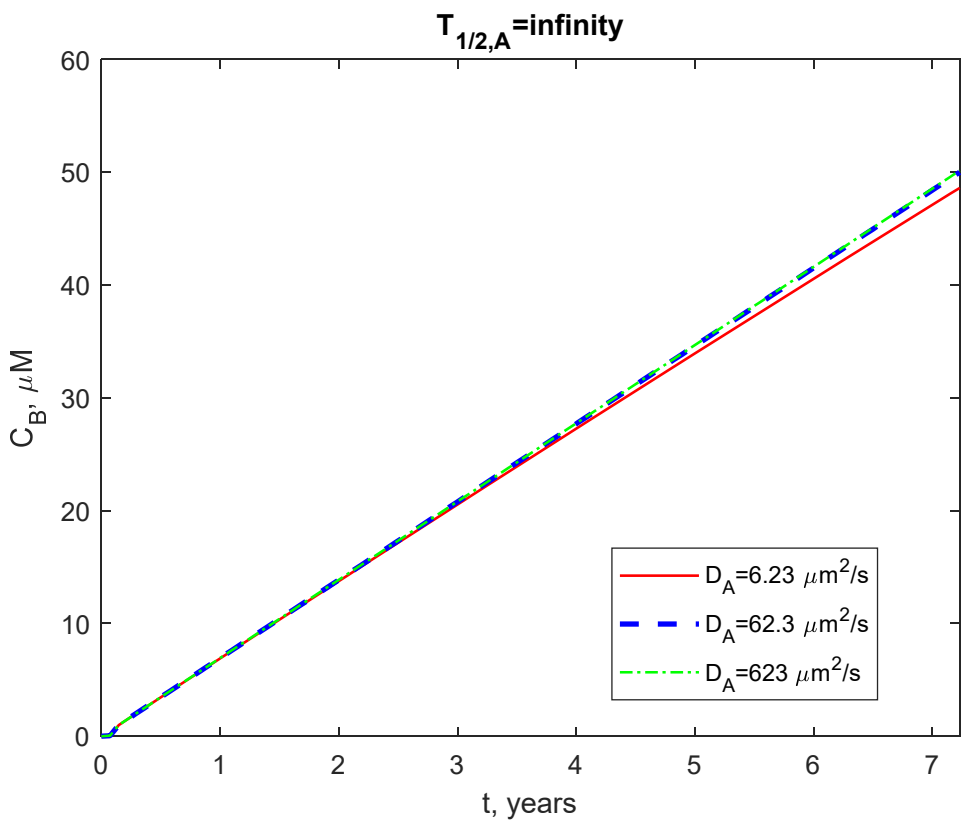
T1/2,A=infinity
60
50
40
30
20
10
0
CB, μM
0
1
2
3
4
5
6
7
t, years
DA=6.23 μm2/s
DA=62.3 μm2/s
DA=623 μm2/s

Figure 3

(a)

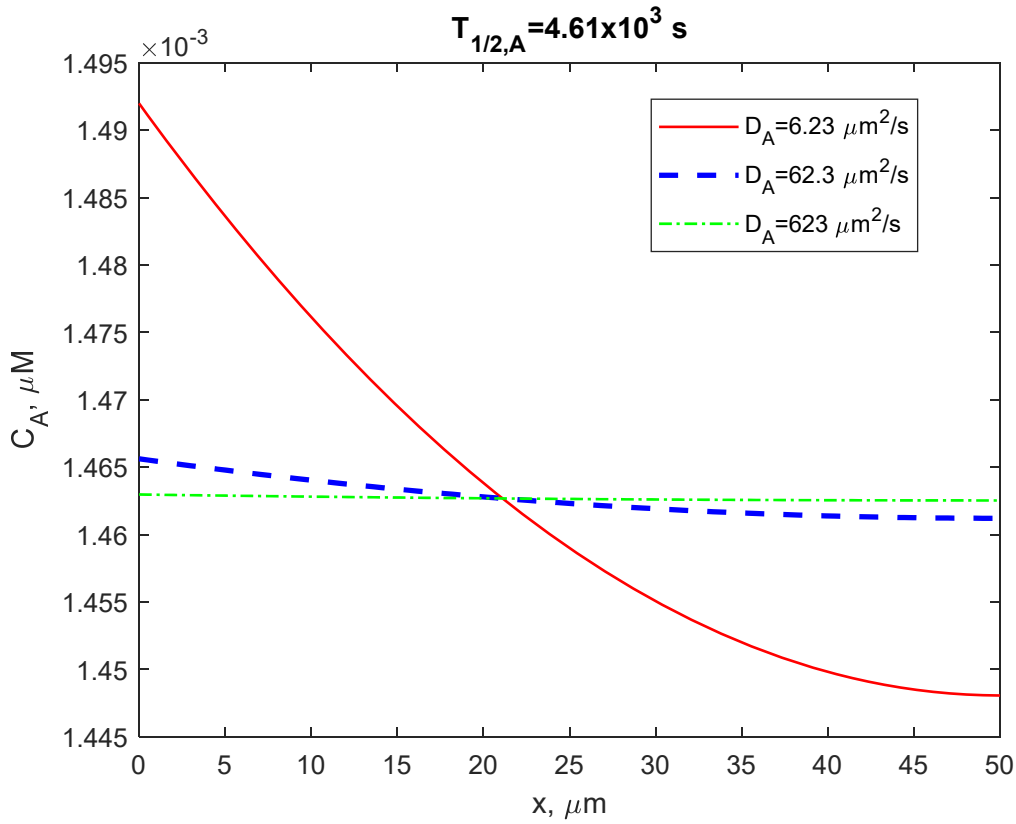
T1/2,A=4.61x10^3 s
×10^-3
1.495
1.49
1.485
1.48
1.475
1.47
1.465
1.46
1.455
1.45
1.445
CA, μM
0
5
10
15
20
25
30
35
40
45
50
x, μm
DA=6.23 μm2/s
DA=62.3 μm2/s
DA=623 μm2/s

(b)

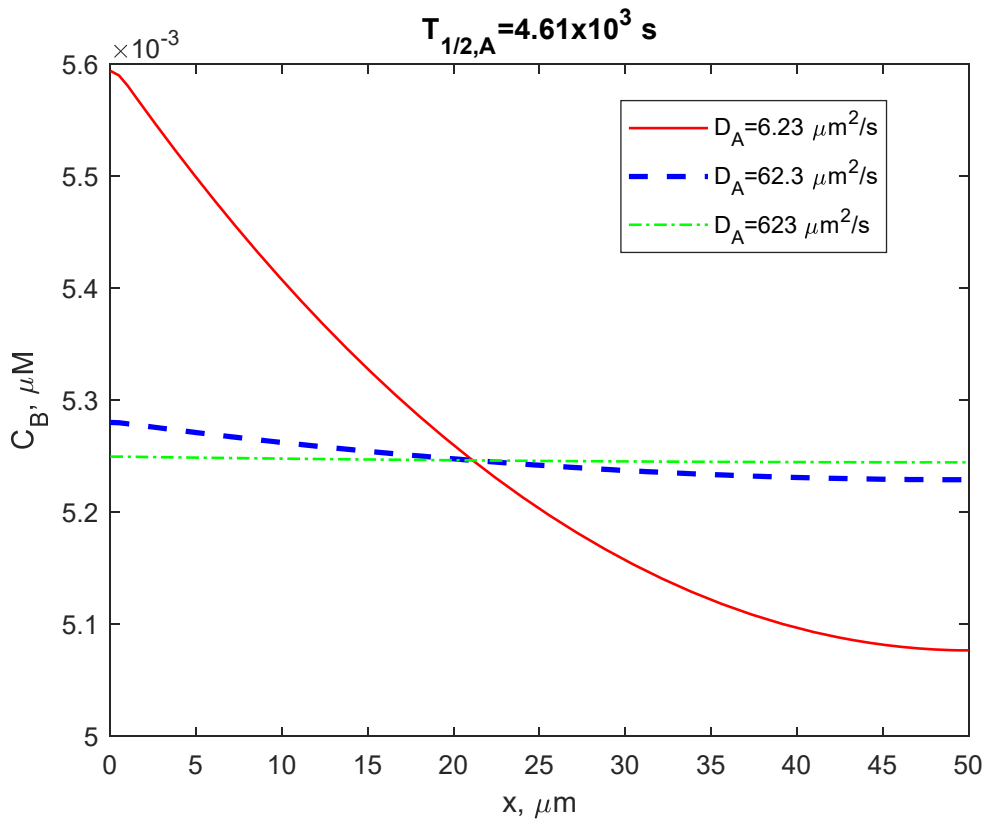
T1/2,A=4.61x10^3 s
×10^-3
5.6
5.5
5.4
5.3
5.2
5.1
5
CB, μM
0
5
10
15
20
25
30
35
40
45
50
x, μm
DA=6.23 μm2/s
DA=62.3 μm2/s
DA=623 μm2/s

Figure 4

(a)

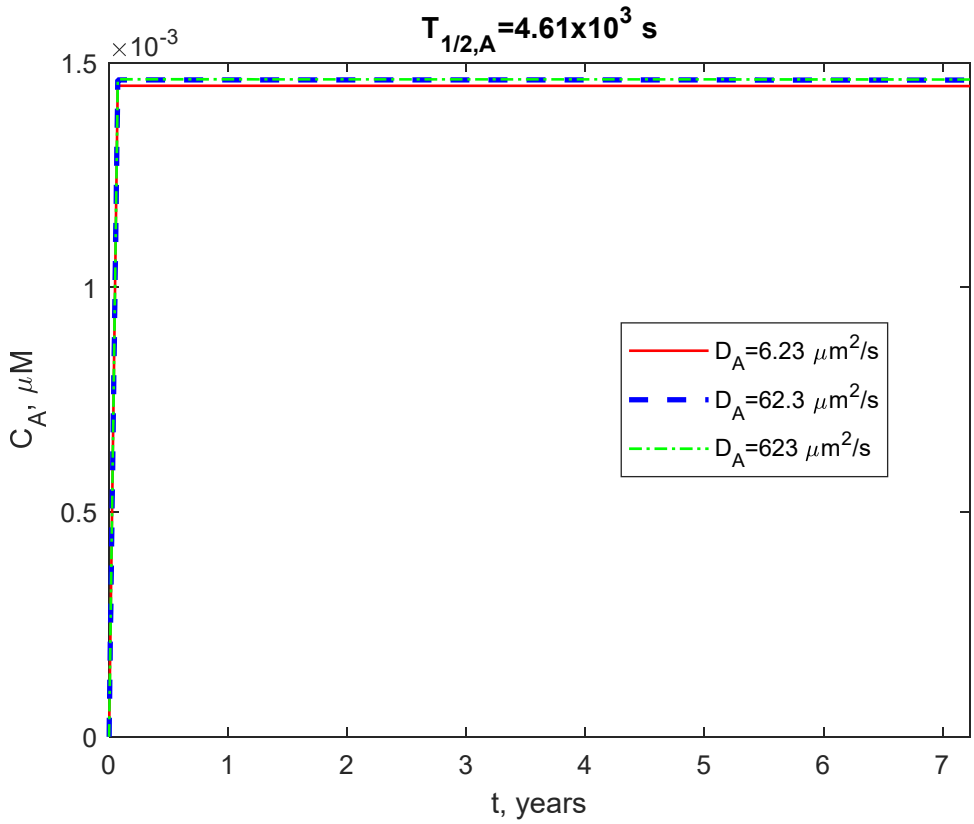
T1/2,A=4.61x10^3 s
×10^-3
1.5
1
0.5
0
CA, μM
0
1
2
3
4
5
6
7
t, years
DA=6.23 μm2/s
DA=62.3 μm2/s
DA=623 μm2/s

(b)

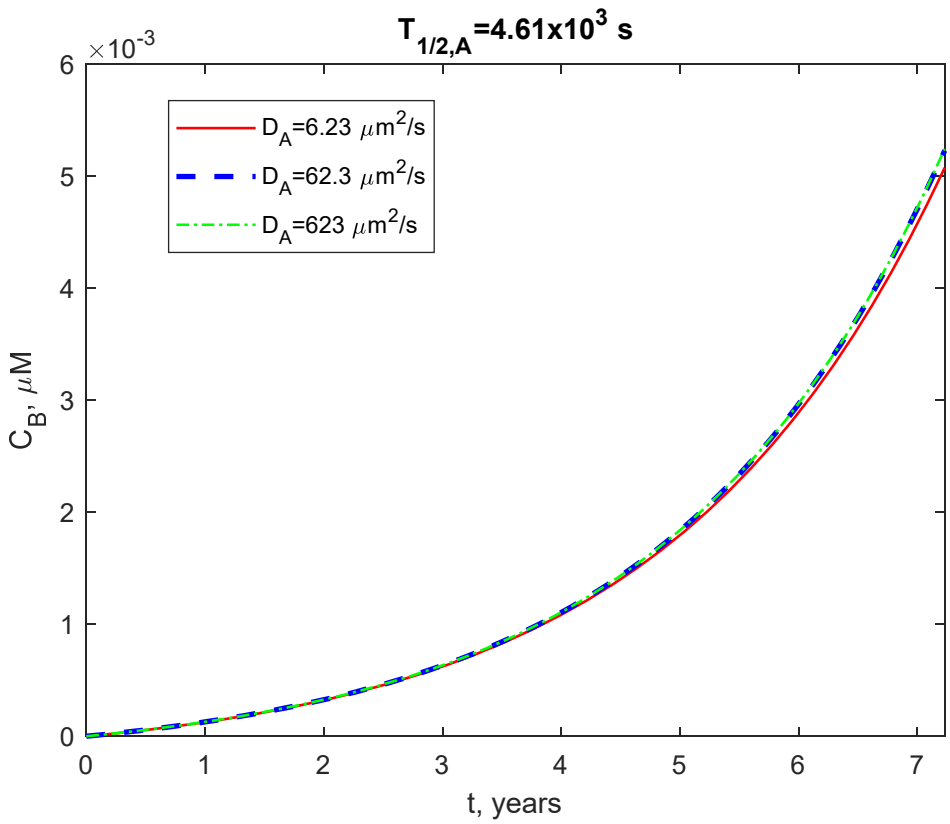
T1/2,A=4.61x10^3 s
×10^-3
6
5
4
3
2
1
0
CB, μM
0
1
2
3
4
5
6
7
t, years
DA=6.23 μm2/s
DA=62.3 μm2/s
DA=623 μm2/s

Figure 5

(a)

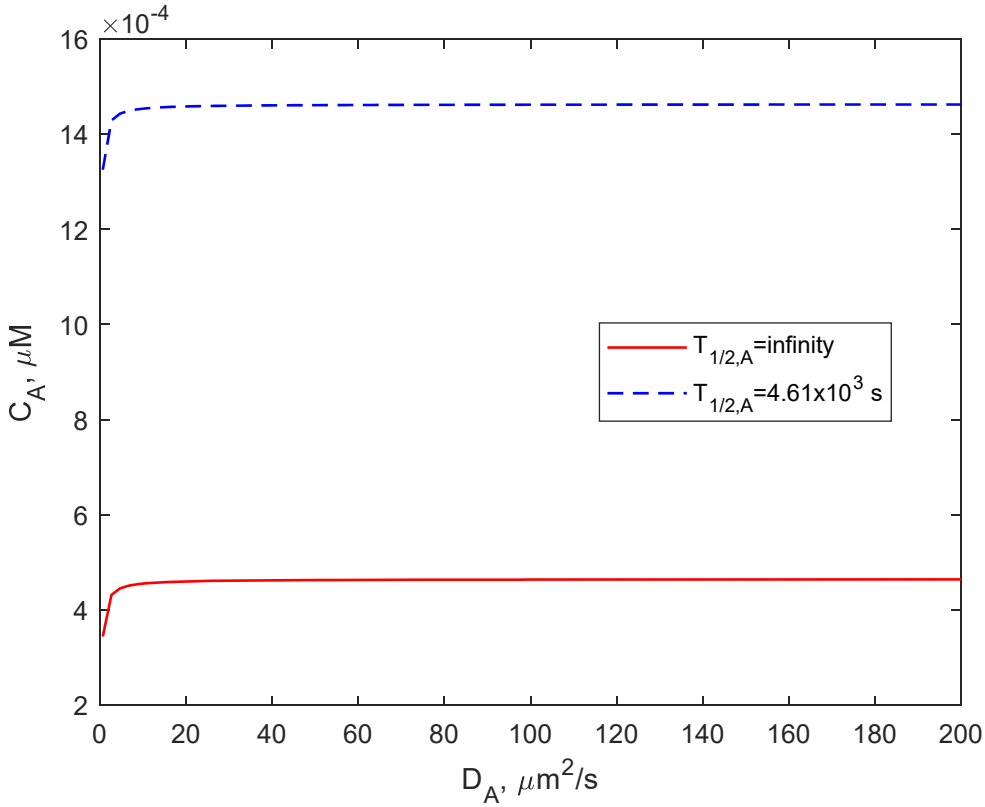
×10^-4
16
14
12
10
8
6
4
2
C_A, μM
0
20
40
60
80
100
120
140
160
180
200
D_A, μm^2/s
T_1/2,A=infinity
T_1/2,A=4.61x10^3 s

(b)

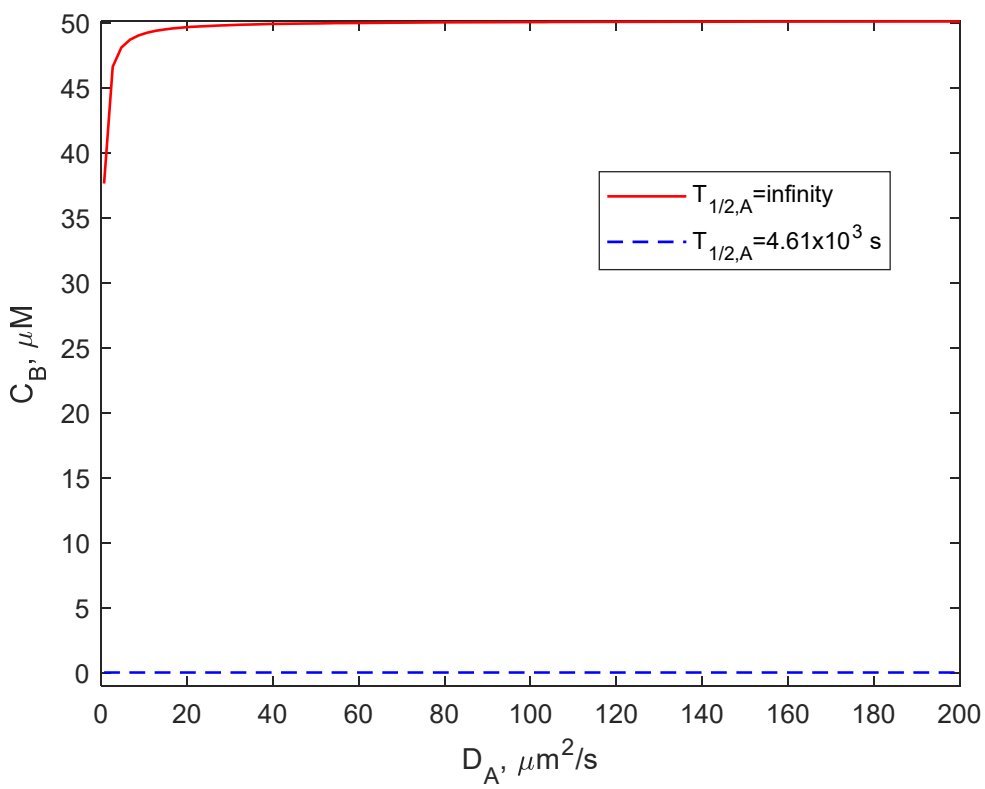
50
45
40
35
30
25
20
15
10
5
0
C_B, μM
0
20
40
60
80
100
120
140
160
180
200
D_A, μm^2/s
T_1/2,A=infinity
T_1/2,A=4.61x10^3 s

Figure 6

(a)

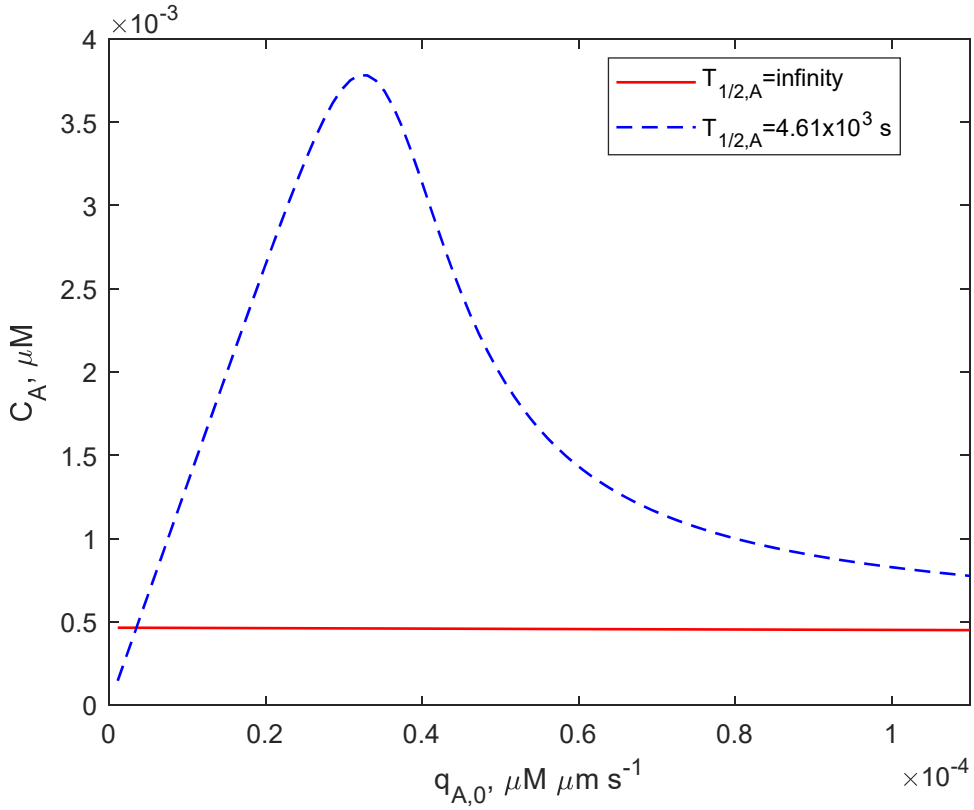
×10^-3
4
3.5
3
2.5
2
1.5
1
0.5
0
C_A, μM
0
0.2
0.4
0.6
0.8
1
×10^-4
q_A,0, μM μm s^-1
T_1/2,A=infinity
T_1/2,A=4.61x10^3 s

(b)

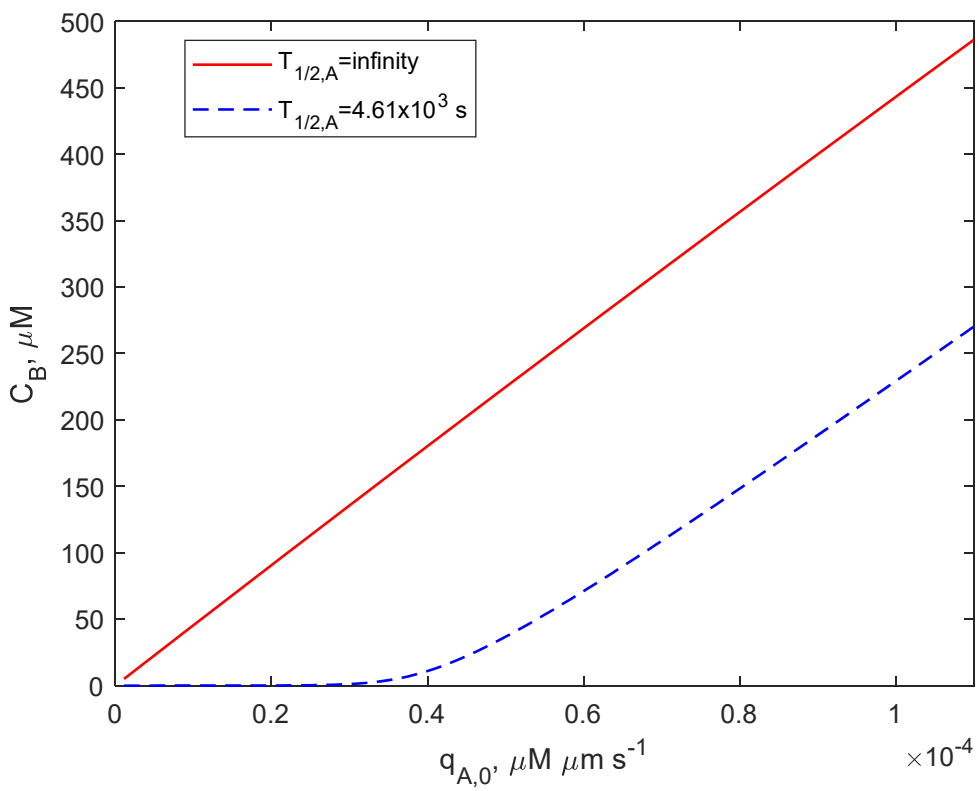
500
450
400
350
300
250
200
150
100
50
0
C_B, μM
0
0.2
0.4
0.6
0.8
1
×10^-4
q_A,0, μM μm s^-1
T_1/2,A=infinity
T_1/2,A=4.61x10^3 s

Figure 7

(a)

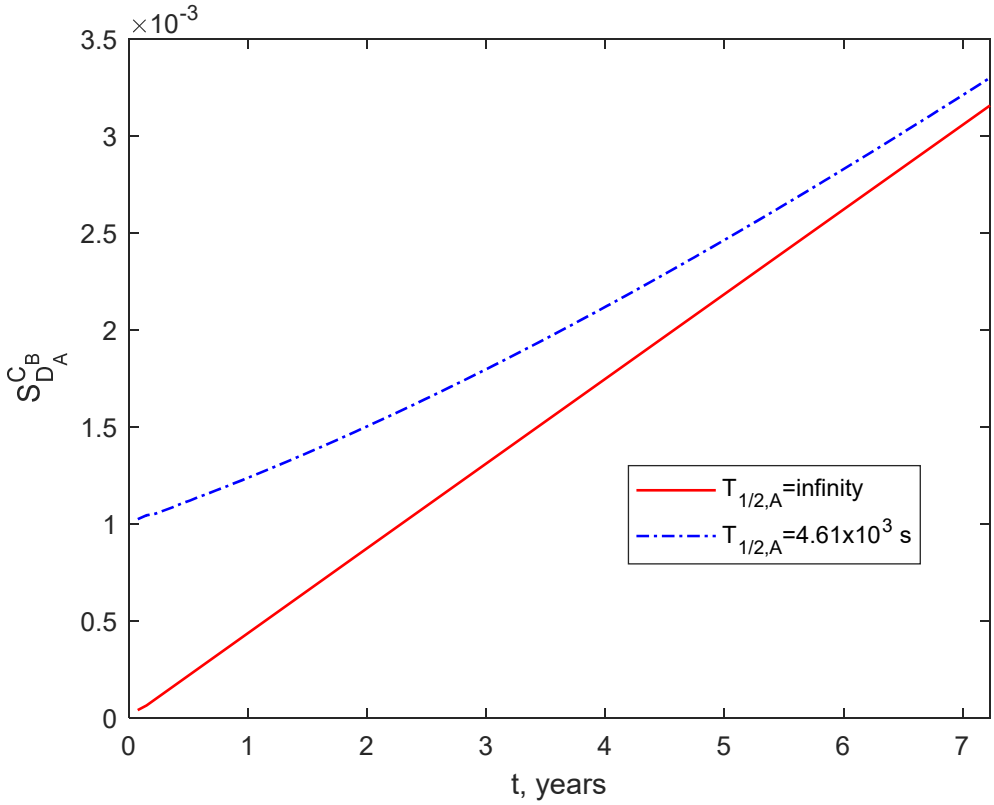
×10^-3
3.5
3
2.5
2
1.5
1
0.5
0
0
1
2
3
4
5
6
7
t, years
$S^{C_B}_{D_A}$
T 1/2,A=infinity
T 1/2,A=4.61x10^3 s

(b)

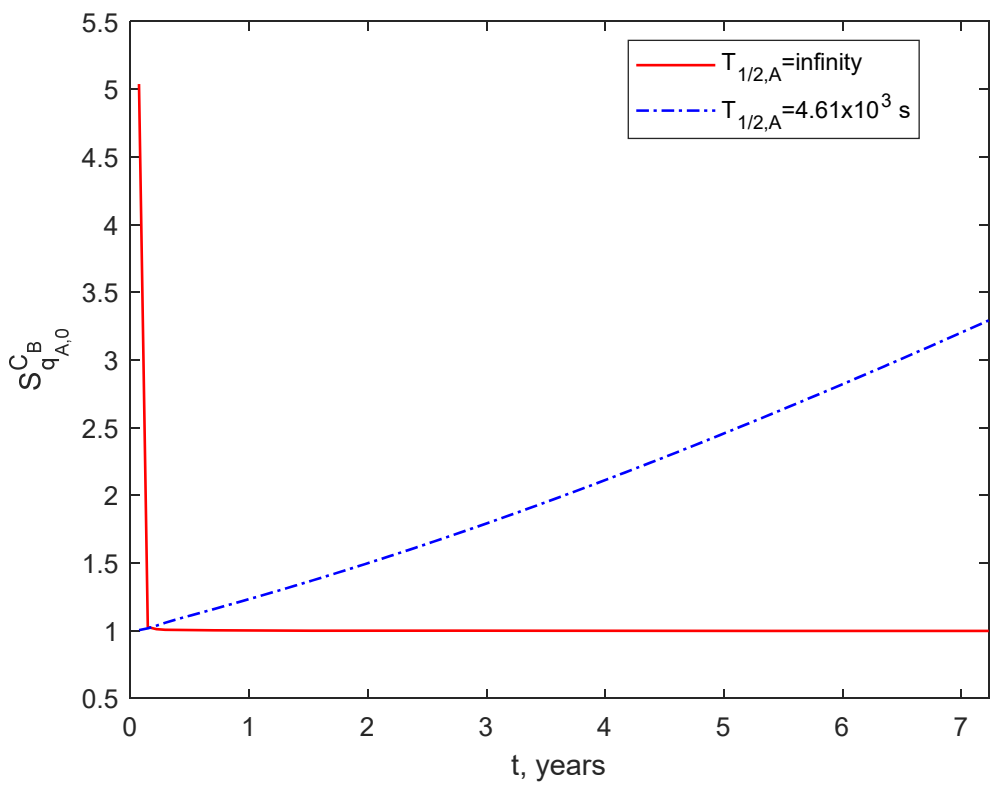
5.5
5
4.5
4
3.5
3
2.5
2
1.5
1
0.5
0
1
2
3
4
5
6
7
t, years
$S^{C_B}_{q_{A,0}}$
T 1/2,A=infinity
T 1/2,A=4.61x10^3 s

Figure 8

**Effect of diffusivity of amyloid beta monomers on the formation of senile plaques**

Andrey V Kuznetsov

Department of Mechanical and Aerospace Engineering, North Carolina State University,

Raleigh, NC 27695-7910, USA; e-mail: avkuznet@ncsu.edu

## Supplemental Materials

### S1. Dimensionless equations

### S1.1. Dimensionless form of Eqs. (3)-(7)

The model represented by Eqs. (1)-(7) is reformulated in its dimensionless form as follows:

$$\frac{\partial C_A^*}{\partial t^*} = D_A^* \frac{\partial^2 C_A^*}{\partial x^{*2}} - C_A^* - C_A^* C_B^* - C_A^* \frac{\ln(2)}{T_{1/2,A}^*}, \tag{S1}$$

$$\frac{\partial C_B^*}{\partial t^*} = C_A^* + C_A^* C_B^*, \tag{S2}$$

$$\text{At } t^* = 0: \; C_A^* = 0, \; C_B^* = 0, \tag{S3}$$

$$\text{At } x^* = 0: \; D_A^* \frac{\partial C_A^*}{\partial x^*} = q_{A,0}^*, \tag{S4}$$

$$\text{At } x^* = L^*: \; \frac{\partial C_A^*}{\partial x^*} = 0. \tag{S5}$$

### S1.2. Dimensionless form of Eqs. (8) and (9)

The dimensionless form of Eqs. (8) and (9) is as follows:

$$\frac{dC_A^*}{dt^*} = -C_A^* - C_A^* C_B^* - C_A^* \frac{\ln(2)}{T_{1/2,A}^*} + q_{A,0}^*, \tag{S6}$$

$$\frac{dC_B^*}{dt^*} = C_A^* + C_A^* C_B^*. \tag{S7}$$

Eqs. (S6) and (S7) should be solved with the initial conditions provided in Eq. (S3).

**S1.3. Dimensionless form of Eqs. (16) and (17)**

The dimensionless form of Eqs. (16) and (17) is as follows:

$$C_A^* = \frac{q_{A,0}^*}{1 + q_{A,0}^* t^*}, \tag{S8}$$

$$C_B^* = q_{A,0}^* t^* . \tag{S9}$$

**S2. Tables**

Table S1. Dimensionless independent variables used in the model.

| Symbol | Definition |
|---|---|
| $t^*$ | $t k_1$ |
| $x^*$ | $x / L$ |

Table S2. Dimensionless dependent variables used in the model.

| Symbol | Definition |
|---|---|
| $C_A^*$ | $C_A k_2 / k_1$ |
| $C_B^*$ | $C_B k_2 / k_1$ |

Table S3. Dimensionless parameters used in the model.

| Symbol | Definition | Value(s) obtained using the dimensional parameter values provided in the last column of Table 3 |
|---|---|---|
| $D_A^*$ | $D_A / \left(L^2 k_1\right)$ | $1.12 \times 10^7$ |

| | | |
|---|---|---|
| $q^*_{A,0}$ | $q_{A,0}k_2 / \left(k_1^2 L\right)$ | $4.21\times10^5$ |
| $T^*_{1/2,A}$ | $T_{1/2,A}k_1$ | $1.02\times10^{-5}$ , $1.02\times10^{1}$ (to represent $T^*_{1/2,A}\to\infty$) |

**S3. Supplementary figures**

(a)

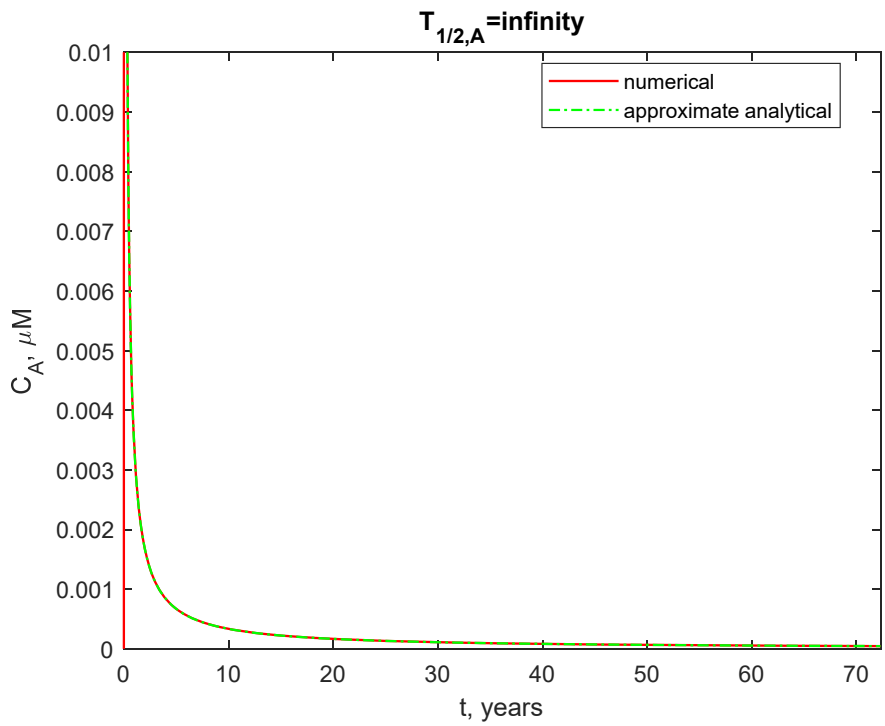

(b)

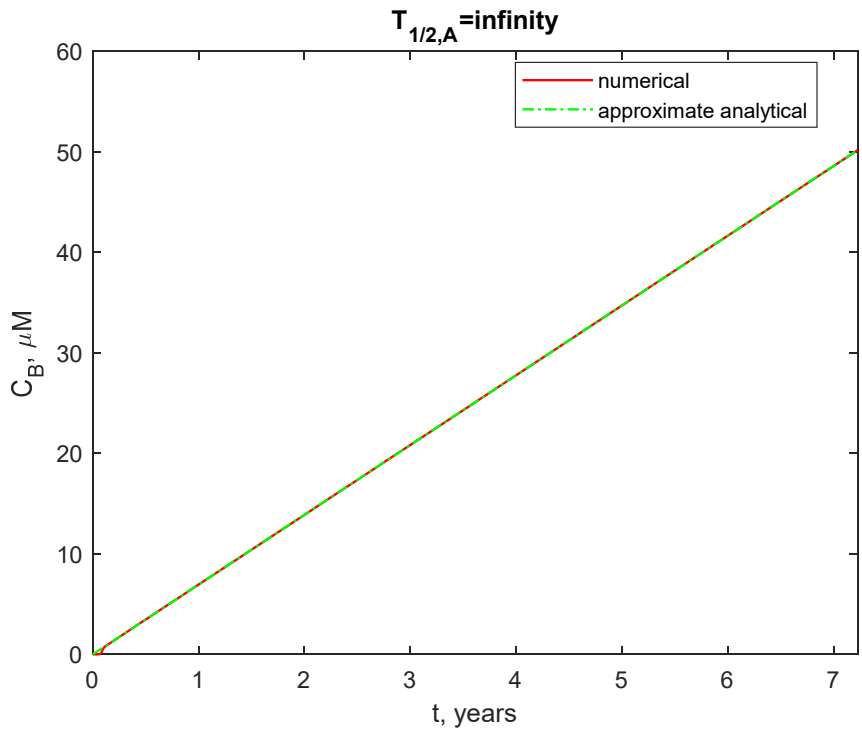


Fig. S1. A comparison between the numerical solutions of Eqs. (8) and (9) and the approximate solutions given by Eqs. (16) and (17). (a) Molar concentration of Aβ monomers, $C_A$, as a function of time (in years). (b) Molar concentration of Aβ aggregates, $C_B$, as a function of time (in years).

(a)

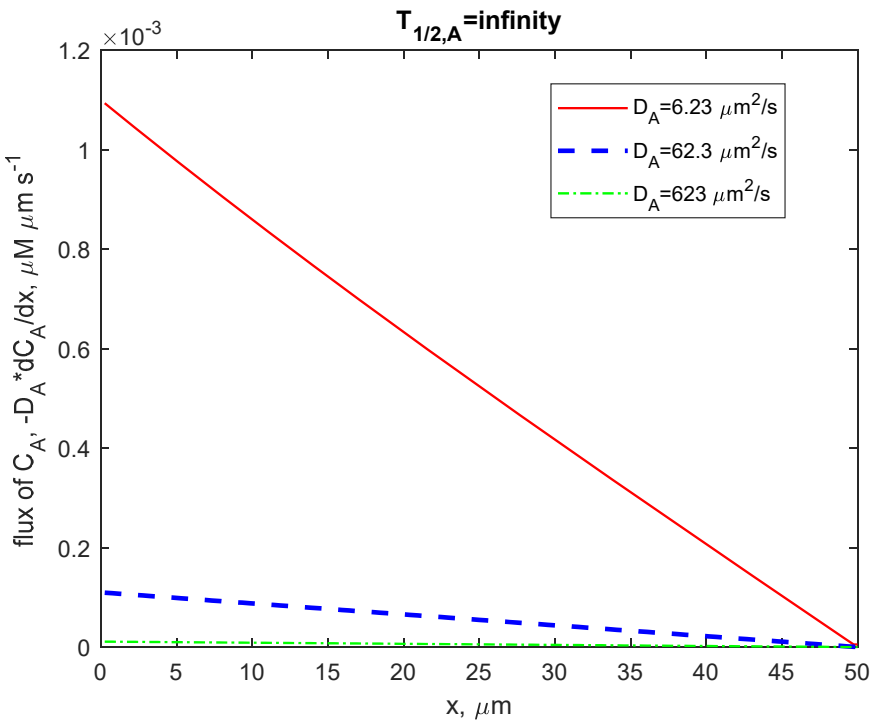
T1/2,A=infinity
×10-3
1.2
1
0.8
0.6
0.4
0.2
0
0
5
10
15
20
25
30
35
40
45
50
x, μm
flux of CA, -DA*dCA/dx, μM μm s-1
DA=6.23 μm2/s
DA=62.3 μm2/s
DA=623 μm2/s

(b)

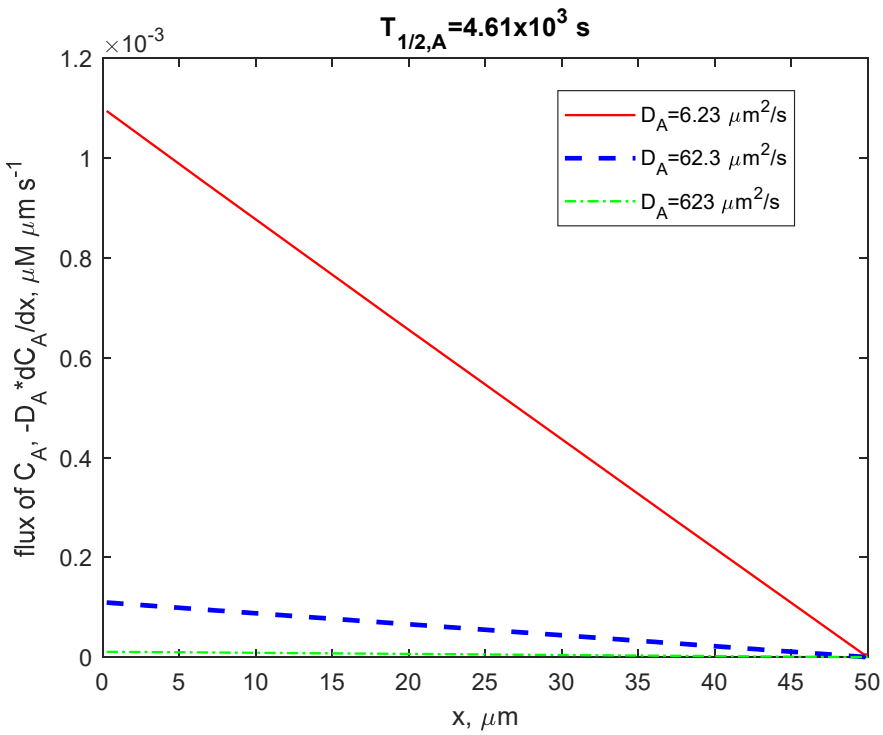
T1/2,A=4.61x103 s
×10-3
1.2
1
0.8
0.6
0.4
0.2
0
0
5
10
15
20
25
30
35
40
45
50
x, μm
flux of CA, -DA*dCA/dx, μM μm s-1
DA=6.23 μm2/s
DA=62.3 μm2/s
DA=623 μm2/s

Fig. S2. Flux of Aβ monomers as a function of the distance from the surface that releases Aβ monomers (such as the cell membrane). The two panels display the results for two different scenarios: (a) $T_{1/2,A} = \infty$, (b) $T_{1/2,A} = 4.61 \times 10^3$ s. The computational results are presented at $t = 2.28 \times 10^8$ s $= 7.23$ years.

(a)

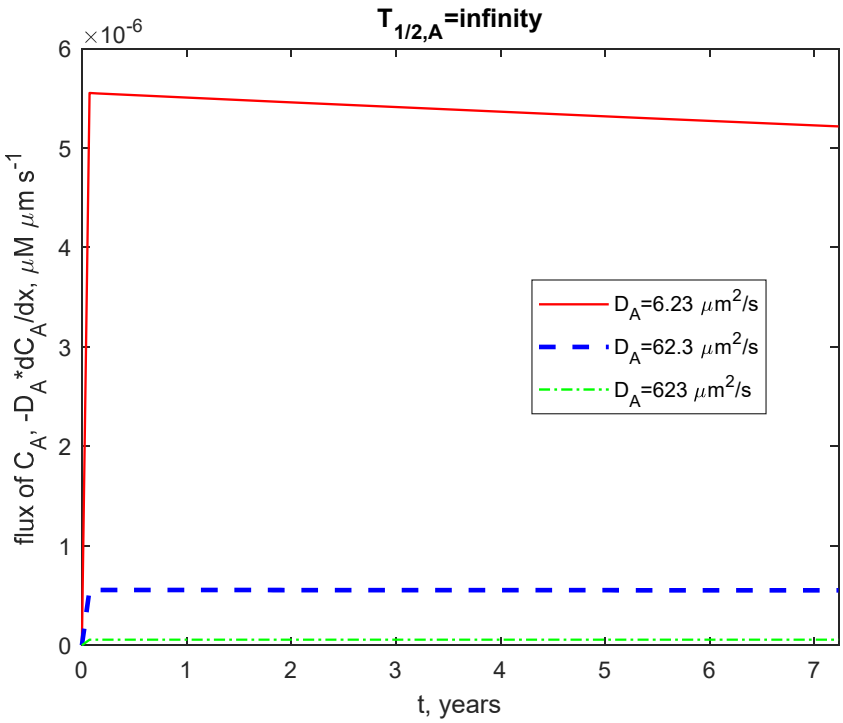

(b)

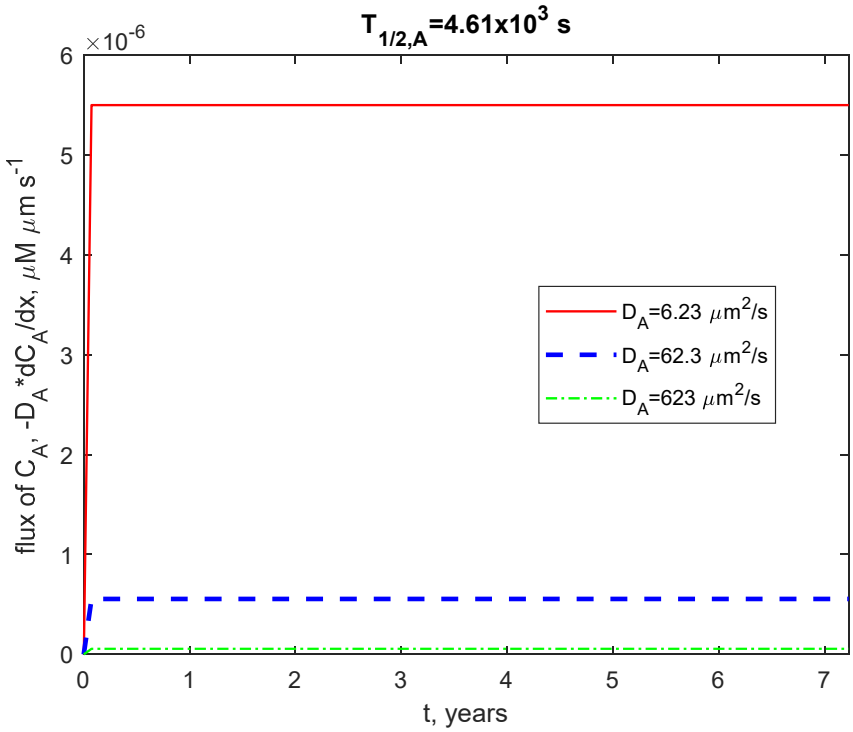


Fig. S3. Flux of Aβ monomers as a function of time (in years). The two panels display the results for two different scenarios: (a) $T_{1/2,A} = \infty$, (b) $T_{1/2,A} = 4.61 \times 10^3$ s. The computational results are presented at the right-hand side boundary of the CV (at $x$=$L$).